Desalination and Water Treatment
www.deswater.com

doi: 10.5004/dwt.2019.23260

138 (2019) 301–312
January

Adsorption kinetics and thermodynamics of Methylene Blue by HKUST-1

R. Sabouni*, A. Aidan, A. AlObeidli, F. Lahib, H. Husni Bacha, R. Kassermally, S. Jarmakani

Department of Chemical Engineering, American University of Sharjah, P.O. Box: 26666, Sharjah, United Arab Emirates, emails: rsabouni@aus.edu (R. Sabouni), aidan@aus.edu (A. Aidan), g00053907@alumni.aus.edu (A. AlObeidli), g00053138@alumni.aus.edu (F. Lahib), b00051888@aus.edu (H.H. Bacha), g00052543@aus.edu (R. Kassermally), g00052976@aus.edu (S. Jarmakani)

Received 7 February 2018; Accepted 9 October 2018

ABSTRACT

The removal of Methylene Blue (MB) from water samples was successfully achieved with high efficiency of 94.2% at 298 K after 60 min using Basolite C300 (or HKUST-1) as a new class of emerging adsorbent called metal organic frameworks. The effect of different experimental parameters, namely dye concentration (50, 150, 200, and 300 mg/L), adsorbent dosage (50, 100, and 150 mg), and temperature (298, 313, and 323 K) was investigated. The adsorption of MB onto HKUST-1 was confirmed using several characterization tests including X-ray diffraction, scanning electron microscope, energy dispersive X-Ray analyzer, Fourier transform infrared spectroscopy, and thermogravimetric analysis. The Langmuir and Freundlich isotherm models were applied to correlate the adsorption isotherms. Although the experimental data fit both models, the Langmuir model is more suitable for higher adsorbent dosage while the Freundlich model is better for lower adsorbent dosage. Based on the Langmuir isotherm, the maximum adsorption capacity of MB onto HKUST-1 reached 250 mg/g. Furthermore, the adsorption kinetic studies showed that the pseudo-second-order kinetic model yields the best fit for the kinetic data with a regression constant, R^2, of (0.9916 to 0.9998). The thermodynamic studies revealed that the process is exothermic (ΔH° = –112.172 kJ/mol) and spontaneous (ΔG° negative) in nature.

Keywords: Adsorption; Methylene Blue; Isotherm; Kinetics; Thermodynamics; Metal organic frameworks (MOFs)

1. Introduction

Wastewater treatment is defined as the treatment of any type of water that has been used industrially or has been flushed from homes or businesses and is no longer fit for reuse as it is contaminated. The process of wastewater treatment is an evolving study which was originally divided into primary, secondary, and tertiary sectors. Today, a challenge for the scientific community which can be named as the fourth type of wastewater treatment, is the removal of micropollutants. "Micro" refers to the pollutants' molarity, as they are present in trace concentrations ranging between 1 ng/L to 1 μg/L. Micropollutants are also known as "emerging contaminants", as they are compounds that emerged from pharmaceutical, pesticide, textile, and many other industries and compounds. Overall, the diversity and relatively low concentration of micropollutants complicate detection and treatment processes [1,2].

The effects of micropollutants include heartbeat increase in humans, tissue necrosis in both humans and animals, and higher chance of mammary tumors in animals [1,3,4]. In addition, guidelines and regulations for the amount of micropollutant present in effluents are not set in most wastewater treatment plants and other industries such as the pharmaceutical and textile industry [5]. For instance, the world dye industry loses 15% of its production as waste liquid effluent containing micropollutants. This waste liquid effluent contains extremely small concentrations of toxic

* Corresponding author.

contaminants. However, due to the excessive amounts disposed and the high accumulation effect that is taking place, these colored wastes can have a significant long-term effect on the ecosystem. As dyes cannot be removed easily due to their synthetic origin and complex aromatic molecular structures; they result in stable non-biodegradable compounds. Current conventional wastewater treatments techniques including biodegradation [6], coagulation [7], sedimentation, and filtration [8] are insufficient and ineffective in solving the problem. In addition, and beside their high energy demand, conventional techniques can result in production of toxic sludge [9].

Methylene Blue (MB) is an organic industrial dye that is not readily biodegradable. Even though it is used in the medical field to treat abnormal hemoglobin, it can cause heart disease, high blood pressure, and lack of muscle coordination [10]. The proposed advanced treatments to remove these compounds from drinking water are systems based on adsorption, ozonation, photodegradation, and membrane filtration [11]. Among those, adsorption has been proven to be a promising solution owing to its high efficiency, simplicity, cost-effectiveness, and ease of handling [12].

Ozonation technique usually requires high capital, operation, and maintenance costs as it includes complex processes such as the ozone destructive unit and deep contact chambers [13]. As demonstrated by Kasprzyk-Hordern et al. [14], one of the main limitations of ozonation is the post-ozonation treatment processes that are required. Besides partially oxidizing micropollutants, ozonation reactions often result in the formation of toxic byproducts such as carbonyl compounds, and keto and carboxylic acids, which are proven to be carcinogenic [15].

Photocatalysis suffers from some technical barriers limiting its application in large-scale processes such as low adsorption capacity for hydrophobic contaminants, regeneration of the catalyst, and difficulty of maintaining uniform distribution of aqueous suspension [16].

On the other hand, adsorption is used universally as it can be utilized for the removal of soluble, insoluble, organic, and inorganic pollutants, with an efficiency of 90%–99%, while being fast and economical. The process of adsorption is dependent on many factors, including temperature, presence of other micro-pollutants, and experimental conditions, such as pH, concentration, particle size of adsorbent, and the contact time between the adsorbate and adsorbent. A wide range of adsorbents have been used for the removal of various contaminants such as dyes, metal ions, pharmaceutical compounds, and pesticides from aqueous solutions. For example, the removal of MB from aqueous solutions has been investigated using activated carbon [12,17,18], zeolite [19], coconut leaf [20], pineapple leaf powder [21], and others. Although activated carbon is the most widely used adsorbent for the removal of MB, there is a need and a great potential for exploring new advanced adsorbent materials such as metal organic frameworks (MOFs).

MOFs emerged as a new class of crystalline porous materials that have possible industrial applications in gas separation, adsorption and storage processes [22], heterogeneous catalysis [23], pharmaceutical manufacturing processes, and drug delivery carriers [24]. Although there have been few publications on using MOFs for the removal of dyes from wastewater, they gained significant interest as promising adsorbents, due to their outstanding properties. These properties include high specific surface area and pore volume, highly diverse structural chemistry [25], and tuneable pore size from microporous (i.e., <2 nm) to mesoporous (i.e., 2–50 nm) scale [26]. Researchers have reported the use of MOFs such as SCU-101, SCU-8, SZ-2, and SZ-3 for the removal of several environmental pollutants [26–28]. SCU-101 and SCU-8 both exhibited fast removal kinetics toward TcO_4^- and perfluorooctane sulfonate (PFOS), respectively [27,28]. Moreover, SZ-2 and SZ-3 achieved effective removal of uranyl ions from aqueous solutions over a wide pH range [29].

Shi et al. [30] investigated the removal of MB using Ni-MOF. Based on their study, they found that adsorption rate could reach 85.08%. Another study performed by Haque et al. [31] has shown that adsorption capacity of MOF-235 is much higher than activated carbon and the adsorption is spontaneous. The adsorptive behavior of MB onto Uio-66 was investigated by Mohammadi et al. [32]. It was found that the maximum adsorption capacity of UiO-66 for MB was 91 mg/g. MIL-8 MOF has been studied by Saghanejhad Tehrani and Zare-Dorabei [33]. It was found that the MB adsorption kinetics fits best the pseudo-second-order model. Consequently, MOFs have been shown as very promising candidates for the removal of MB from aqueous solutions.

Dye adsorption is a relatively complex mechanism as it depends, to a large extent, on the surface free energy interaction. However, studying the adsorption kinetics and thermodynamic properties provide an insight on the mechanism of adsorption. As previously investigated by Gooding et al. [34], the adsorption mechanism and the rate at which the dye molecules are transferred to the adsorbent can be described by the following: (1) transport of dye through the bulk solution to the surface of the adsorbent, (2) adsorption of the dye molecule onto the surface of the adsorbent, (3) diffusion of the dye from the surface to the interior of the adsorbent.

The main objective of this research paper is to investigate the adsorption kinetics and thermodynamics of MB onto HKUST-1. As well as to perform a parametric study on the adsorption efficiency of HKUST-1 under several experimental parameters including MB initial concentration (50, 150, 200, 300 mg/L), adsorbent dosage (50, 100, 150 mg), and temperature (298, 313, and 323 K). A study of the adsorption isotherm models of MB onto HKUST-1 and the thermodynamic properties including ΔH (kJ/mol), ΔS (kJ/mol K), and ΔG (kJ/mol) is also conducted. Therefore, the objective of this paper is to thoroughly discuss the process of adsorption both experimentally and thermodynamically such that a justifiable conclusion is achieved on the efficiency of MOFs in MB adsorption.

2. Materials and methods

All chemicals were used without further modifications. Methylene Blue (MB), supplied by LABCO (the official Sigma-Aldrich distributor in the United Arab Emirates), was chosen as the micropollutant for the adsorption experiments. MB has a chemical formula of $C_{16}H_{18}ClN_3S$ and molecular weight of 319.85 g/mol. A stock solution of 15 g/L was prepared and stored for further dilution to prepare the required studied concentrations of (50, 100, 150, and 300 mg/L). The adsorbent

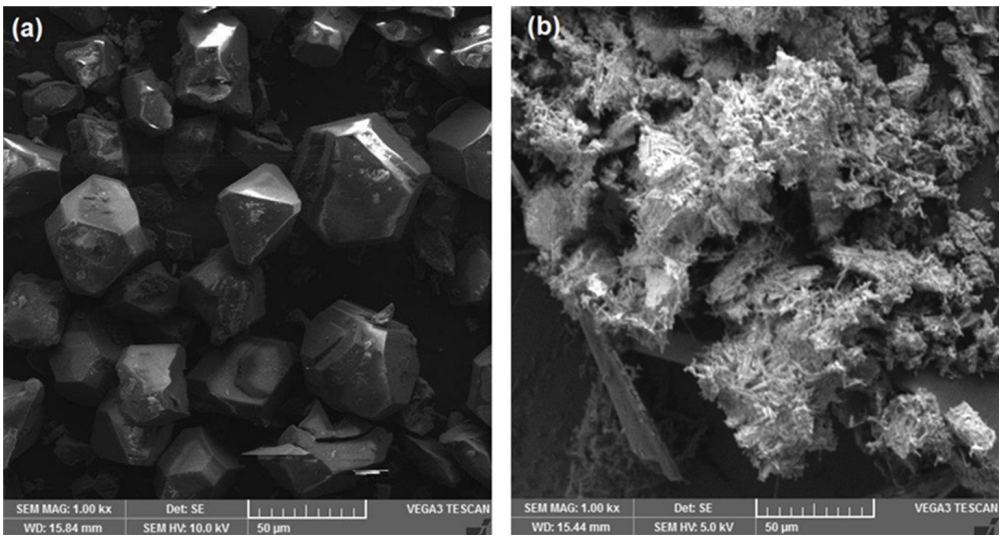

Fig. 1. SEM images of HKUST-1 (a), HKUST-1 after adsorption of MB (b).

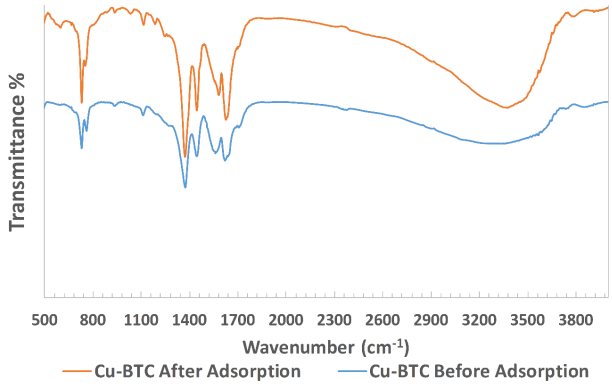

Fig. 2. FTIR patterns for HKUST-1 and HKUST-1 after adsorption of MB.

studied in this paper is HKUST-1 (Basolite C300 from Sigma-Aldrich). It has a molecular weight of 604.87 g/mol, a particle size of 15.96 µm, and a surface area of 1,500–2,100 m^2/g based on Brunauer–Emmett–Teller data.

The concentration of MB in the tested samples was measured using APEL PD 303S UV Spectrophotometry at λ_{max} of 664 nm. A calibration curve for MB was obtained from the spectra of diluted solutions.

A number of characterization tests were performed for HKUST-1 before and after adsorption of MB including scanning electron microscope–energy dispersive X-Ray (SEM-EDX), FTIR, TGA, and X-ray diffraction (XRD). The morphology and crystal structure of HKUST-1 was studied by SEM. The SEM-EDX images were taken by (VEGA III XMU with Oxford X-Max 50 EDS) operating at 10 keV of acceleration voltage as shown in Fig. 1. The Fourier transform infrared spectroscopy (FTIR) measurements were performed using Spectrum one FTIR spectrometer (as shown in Fig. 2). To investigate the thermal stability of HKUST-1 before and after adsorption, The XRD spectra were recorded using D8 Advance diffractometer (Bruker, Germany) using a Cu Ka (k = 1.54 Å) radiation source on a silicon wafer from 3° to 40° (2θ) with a step size of 0.02° and 1 s (per step) in

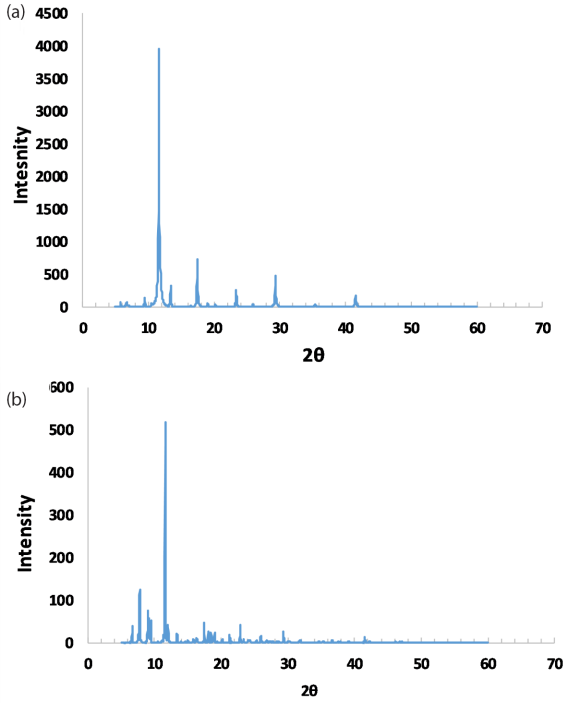

Fig. 3. XRD patterns for HKUST-1 (a) and HKUST-1 after adsorption of MB (b).

a continuous mode (Fig. 3). To investigate the thermal stability of HKUST-1, thermogravimetric analysis (TGA) was performed using PerkinElmer (Germany) TGA system with heating rate of 15°C/min from 30°C to 700°C (Fig. 4).

3. Experimental procedure

3.1. Adsorption

In order to investigate the adsorption kinetics and thermodynamic behavior of HKUST-1 for MB in aqueous solution, exact amounts of the adsorbent HKUST-1 (50,

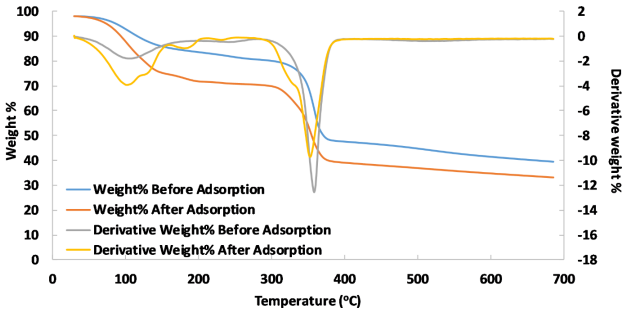

Fig. 4. TGA for HKUST-1 before and after adsorption of MB.

100, and 150 mg) were added to the aqueous MB solution (50 mL) with different concentrations of 50, 150, 200, and 300 mg/L and at different temperatures (298, 313, and 323 K). The mixtures were well mixed with magnetic stirrers over a duration ranging between 5 min and 12 h. The adsorbent was then separated from the solution by a syringe filter (PTFE, hydrophobic, 0.5 μm). The remaining MB in the solution was measured by UV spectrophotometer at the maximum absorption wavelength of 664 nm. The adsorbed amount of MB onto HKUST-1 was calculated by subtracting the amounts of free MB at equilibrium from the initial MB concentration using Eq. (1) [17]:

$$q_t = \left(C_o - C_t\right)\frac{V}{W} \tag{1}$$

The removal efficiency of MB was calculated using Eq. (2) [17]:

$$\text{Removal efficiency}\left(\%\right) = \frac{\left(C_o - C_t\right)}{C_o} \times 100 \tag{2}$$

where C_o and C_t (mg/L) are the liquid-phase concentrations of MB at time = 0 and t, respectively; and V (L) and W (g) are the volume of the solution and the weight of the adsorbent, respectively.

One of the most important issues in the adsorption process is the regeneration and reuse of the used adsorbent. To investigate the regeneration of HKUST-1, the used HKUST-1 samples were washed with methanol and dried in an oven at 100°C for 7 h. Next, the adsorption experiment was repeated, as previously mentioned, for two cycles of 50 mg/L MB initial concentration and 100 mg HKUST-1.

4. Results and discussion

4.1. Characterization tests

To understand the adsorption mechanism of MB onto HKUST-1 samples, several characterization tests were performed. According to Fig. 1(a), HKUST-1 has an octahedral crystal structure which is consistent with previously published SEM image [34]. However, the crystal surface structure and roughness of HKUST-1 after adsorption of MB has been changed indicating the adsorption of MB on the surface of the MOFs (as shown in Fig. 1(b)). This was also confirmed previously in similar studies with different adsorbents [35,36]. The EDX data indicate the element composition of HKUST-1 before adsorption (Fig. S1(a)). After adsorption, the presence of Cl and S elements is another indication of successful adsorption of MB on the surface of HKUST-1 and inside the pores (Fig. S1(b)). The XRD patterns of HKUST-1 before and after adsorption are shown in Fig. 3. The results shown in Fig. 3 confirm the crystallinity of HKUST-1. Comparing with the simulated XRD pattern previously published [37], shown in Fig. S2, most of the significant peaks of HKUST-1 reported in literature are present (i.e., 2θ = 11.61°, 13.4°, 17.45°, 23.36°, and 29.33°) [38]. The main significant difference between the XRD patterns before and after adsorption is the presence of two additional peaks at 2θ = 6.7° and 9.5° and the extent of noise in the after-adsorption sample. This is potentially due to the presence of water and MB in the MOF samples. Furthermore, it can be clearly observed that the HKUST-1 samples have not encountered any change in crystallinity after adsorption, which is an indication that the crystalline structure of HKUST-1 remained stable after adsorption. Fig. 2 represents the FTIR results of HKUST-1 before and after adsorption. The FTIR patterns are in good agreement with the previously published results [39,40].

The main observation is the pronounce presence of water molecules in HKUST-1 after adsorption, which can be identified by the broad peaks between 3,800 and 3,000 cm^{-1} that correspond to the presence of OH group of the adsorbed water molecules. Water molecules in the sample before adsorption are mainly from the moisture in the atmosphere, whereas the water in the sample after adsorption is mainly from the adsorbed water molecule from the aqueous solution. This observation is confirmed in literature [40,41]. Another important difference is the appearance of new peaks at 1,000; 1,171; and 1,295 cm^{-1} and the shift of the peak at 3,747 to 3,792 cm^{-1}. This may be attributed to adsorption of MB onto HKUST-1 [42]. Additionally, the thermal stability of HKUST-1 was studied up to 700°C as shown in Fig. 4. The figure indicates the overall stability of HKUST-1 before and after adsorption of MB, which was reported previously in literature [38]. The first weight loss around 100°C in both samples is attributed to the evaporation of adsorbed water. However, after-adsorption samples of HKUST-1 show more intense weight loss indicating higher water content (around 30% weight lost). The next weight loss is observed at around 350°C. This weight loss corresponds to the total decomposition of benzene tricarboxylic acid BTC linker and CuO as remaining products. Furthermore, the adsorption ability of the surface is determined by an important factor called the point of zero charge (PZC). To define the PZC, 0.1 g of HKUST-1 was added into 0.01 M NaCl solution. The pH from 2–12 was adjusted by the addition of HCL and NaOH. Then the aqueous solution was shaken for 48 h. The change in pH affects the surface ionic charge of adsorbate molecules and adsorbent materials. Fig. S3 shows the point of zero charge (PZC) of pH_{PZC} = 4.2 for HKUST-1. As the pH increased, the surface charge of HKUST-1 became more negative, as a result of the deposition of more OH^- on the HKUST-1 surface. Based on the PZC, the HKUST-1 surface charge is more positive at pH ≤ 4.2, but is more negative at pH > 4.2. Accordingly, the adsorption of MB as MB^+ cation form is favorable at pH > pH_{PZC} and unfavorable at pH < pH_{PZC} [43]. This finding

confirms the high adsorption capacity of MB by HKUST-1 at the specified experimental conditions.

4.2. Kinetics of adsorption

Studying the adsorption kinetics of a process is important as it provides essential information about the uptake rate of adsorbate and the adsorption mechanism such as mass transfer and chemical reaction. To explore the mechanism of MB adsorption onto HKUST-1 and the applicability of pseudo-first and pseudo-second-order kinetic models, the experimental data was fitted to both models by the least squares regression analysis. However, the experimental data followed pseudo-second-order kinetics with a regression constant, R^2, of 0.9916–0.9998, as shown in Table 1. Whereas the pseudo-first-order did not give a good fit to the experimental data. This can be explained as the chemical adsorption might be the rate limiting step in the adsorption process of MB onto HKUST-1.

The pseudo-second-order kinetic model is expressed as Eq. (3) [17]:

$$\frac{t}{q_t} = \frac{1}{k_2 q_e^2} + \frac{1}{q_e} t \tag{3}$$

where q_e (mg/g) is the amount of MB adsorbed at equilibrium, q_t (mg/g) is the amount of MB adsorbed at time t (s), and k_2 (g/mg min) is the pseudo-second-order rate constant. Graphs of t/q_t vs. t for initial concentrations of 50, 150, 200, and 300 mg/L were constructed and the values of q_e and k_2 were obtained from the slope and intercept of the graphs, respectively. The graph of t/q_e vs. t for 50–300 mg/L (MB) and 100 mg of HKUST-1 is shown in Fig. S4; and the R^2 and k_2 values for all initial concentrations are tabulated in Table 1.

Table 1
Values of rate constants of pseudo-second-order constants for removal of MB using HKUST-1

Initial concentration of MB (mg/L)	k_2 (mg/g min)	R^2
50 mg of HKUST-1		
50	49.0	0.9998
150	123.5	0.9985
200	144.9	0.9916
300	196.1	0.9974
100 mg of HKUST-1		
50	26.2	0.9997
150	66.7	0.9993
200	89.3	0.9994
300	126.6	0.9954
150 mg of HKUST-1		
50	17.5	0.9998
150	37.5	0.9989
200	59.2	0.9997
300	95.2	0.9995

4.3. Adsorption mechanism:

The adsorption of MB by HKUST-1 was observed to be rapid at the beginning of the contact time and then becomes slow and reaches a plateau trend with the increase in contact time (Fig. 5). The removal of MB by adsorption on surface of HKUST-1 was due to MB and MB^+ cationic form. Moreover, based on the point of zero charge study at greater pH, the surface of the adsorbent is negatively charged which favors electrostatic interaction of cationic species of the dye with the negatively charged surface. Mathews et al. [44] proposed and explained the mechanism for the removal of dye by adsorption through the following four steps: (1) transport of the dye from the bulk of the solution to the surface of the adsorbent, (2) diffusion of dye through the boundary layer to the surface of the adsorbent, (3) adsorption of dye at an active site on the surface of the adsorbent, and (4) intra-particle diffusion of dye into the interior pores of the particles.

4.4. Effect of initial concentration

The effect of initial concentration of MB on the adsorption capacity and removal efficiency was evaluated at 50, 150, 200, and 300 mg/L. Both the effect of initial concentration and contact time are depicted in Fig. 5. The trend in Fig. 5 clearly shows that percentage removal is strongly affected by the initial concentration of MB. In addition, it was found that as the initial concentration increased from 50 to 300 mg/L, the percentage removal significantly decreased from 94.2% to 69.9% at a contact time of 120 min. Also, all initial concentrations follow the same trend; the removal is very rapid at first with a sharp increase (t = 0–40 min) and then it gradually stabilizes as it reaches equilibrium (t = 120–∞ min). In research done by Albadarin et al. [45], where the adsorption of MB using lignin–chitosan extruded (ALiCE) pellets was investigated, comparable results were obtained. However, when using ALiCE pellets, the adsorption rate only stabilized after 40 h whereas when using HKUST-1, only 120 min were needed for the adsorption rate to stabilize [45]. Moreover, lower the concentration of the pollutant, higher the percentage removal. This is because when the concentration of the pollutant (MB) decreases, the available sites on the adsorbent increase relative to the number of pollutant molecules in the solution. The adsorbent will then be able to adsorb more pollutants on the available sites and thus increase the percentage removal of MB from the solution.

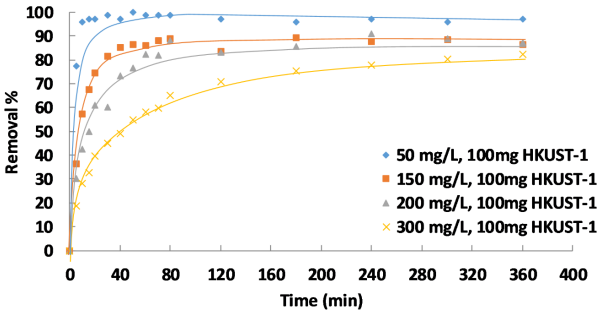

Fig. 5. Effect of initial concentration and contact time (50–300 mg/L) on MB removal at contact time of 360 min and 100 mg HKUST-1.

The regeneration of HKUST-1 was studied for 50 mg/L MB initial concentration and 100 mg HKUST-1 for two cycles. It was found that HKUST-1 MOFs samples can be easily regenerated without significant reduction in removal efficiency after two cycles (92% and 90%, respectively). A similar study has shown that UiO-66 can be regenerated for the removal of MB from aqueous solutions using methanol for multiple times [32].

4.5. Effect of adsorbent dosage

The effect of adsorbent dosage was evaluated at 50, 100 and 150 mg at different initial concentrations of 50, 150, 200, and 300 mg/L as shown in Fig. 6. As initial concentration of MB in a solution increases, the rate of adsorption increases as well. The rate of adsorption is reflective of the adsorption capacity, q_e. Adsorption capacity, q_e, is defined as the accumulation of solute molecules (MB) at the surface of the solid (HKUST-1) hence the units, mg of solute/g of solid or amount of MB absorbed/mass of adsorbent. Adsorption capacity, q_e, is calculated using Eq. (1) [17].

As C_o increases, the concentration gradient ($C_o - C_e$) increases, which increases the rate of diffusion. On the other hand, at any fixed C_o, q_e decreases with increasing adsorbent dosage. In recent research done in 2017 by Sharma et al. [46], the removal of Coomassie brilliant blue R-250 dye using starch/poly(alginic acid-cl-acrylamide) nanohydrogel was studied and similar results were obtained where percentage efficiency increased with adsorbent amount but the amount of dye adsorbed per unit mass (q_e) decreased. This is because the amount of adsorption occurring per unit mass of adsorbent decreases due to the high availability of empty sites following the increase in adsorbent dosage.

Moreover, when using lignin chitosan extruded (ALiCE) pellets, the maximum adsorption capacity obtained was 36.25 mg/g which is similar to the results obtained using HKUST-1 and 50 mg/L of MB. However, when increasing the concentration of MB to 150, 200, and 300 mg/L and using 50 mg of HKUST-1, the adsorption capacity ranged between 130 and 190 mg/g as depicted in Fig. 6 [45]. A comparison of the maximum adsorption capacity of HKUST-1 with other reported adsorbents in literature for adsorption of MB is made in Table 2. The maximum adsorption capacity of MB onto HKUST-1 is 250 mg/g which is the highest adsorption capacity amongst the ones listed in Table 2. This relatively high adsorption capacity can be explained by the high surface area and suitable pore structure of HKUST-1 suggesting that it could serve as a competitive adsorbent due to its availability, cost effectiveness, and efficiency.

4.6. Effect of temperature

The effect of temperature on the adsorption capacity of MB onto HKUST-1 was evaluated at 298, 313, and 323 K for the 150 mg/L solution at an adsorbent dosage of 100 mg of HKUST-1. Fig. 7 shows C/C_o vs. time at different temperatures. C/C_o is another way of representing the removal percentage as it shows the concentration at a certain time divided by the initial concentration. The decreasing trend is due to the removal of MB hence resulting in C/C_o to approach 0. According to Fig. 7, it was observed that the adsorption removal percentage decreases with increasing

Table 2
Comparison of maximum adsorption capacity of MB onto various adsorbents

Adsorbent	Maximum adsorption capacity, q_m (mg/g)	Reference
Waste wool fiber	207.2	[47]
Modified kaolin	111.0	[48]
Activated lignin–chitosan extruded (ALiCE)	36.25	[45]
Brown macroalga	35.06	[49]
UiO-66	91.0	[32]
Mt	64.43	[50]
Fe_3O_4/Mt	106.38	[50]
Propylene diamine basic activated carbons	182.0	[51]
Palm shell-waste based AC	163.3	[52]
Silica hybrid hollow spheres	25.24	[53]
Polydopamine microspheres	88.89	[54]
ZnO/$ZnFe_2O_4$	37.27	[55]
MOF-235	187.0	[56]

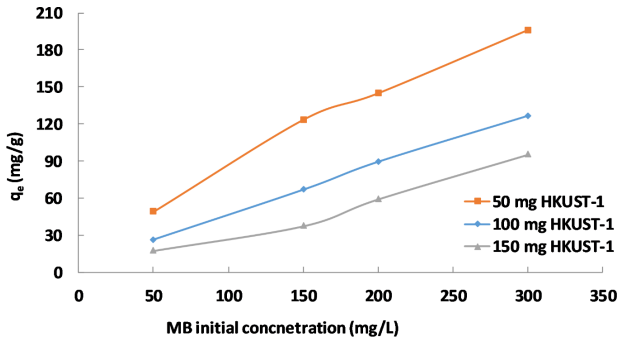

Fig. 6. Effect of adsorbent dosage on the adsorption capacity of MB at different initial concentrations.

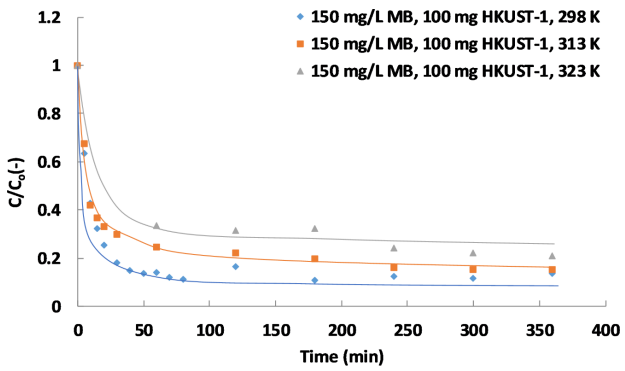

Fig. 7. Effect of temperature on MB removal capacity for 150 mg/L MB and 100 mg HKUST-1.

temperature. When comparing 298 to 323 K at a contact time of 120 min, adsorption removal percentage decreased from 88.1% to 68.2%, respectively.

The decrease in percentage removal with increasing temperature reveals that the adsorption of MB onto HKUST-1 is an exothermic process. This could be due to the fact that at higher temperatures, the solubility increases, and the greater part of the MB remains in the system. Also, given that physical adsorption processes are reversible and exothermic, and following Le Chatelier's principle, an increase in temperature will favor the reversible reaction of adsorption, that is, desorption, which will in turn decrease the adsorption rate. This will be further explained in the following section.

5. Thermodynamics of adsorption

Thermodynamic parameters are useful in better understanding the adsorption mechanism. Parameters such as the thermodynamic equilibrium constant (K_L), the standard Gibbs free energy ($\Delta G°$), standard enthalpy ($\Delta H°$) and standard entropy ($\Delta S°$) were calculated using the following Eqs. (4) and (5) [17]:

$$\ln K_L = \frac{\Delta S°}{R} - \frac{\Delta H°}{RT} \tag{4}$$

$$\Delta G° = \Delta H° - T\Delta S° \tag{5}$$

K_L is the thermodynamic equilibrium constant (unit less). For neutral adsorbates with weak charge, the Langmuir equilibrium constant K_L with units of liters per mole can be reasonably used for determination of $\Delta G°$ [57–60]. R is the universal constant which is equal to 8.314 J/mol K and T is the temperature (K). A linear plot of ln K_L vs. $1/T$ was plotted to obtain the $\Delta S°$ and $\Delta H°$ values from the slope and intercept, respectively. Those values were used to calculate $\Delta G°$ at different temperatures as shown in Table 3. The negative Gibbs free energy ($\Delta G°$) values suggest that the adsorption of MB onto HKUST-1 is spontaneous. Also, the Gibbs energy decreases with increasing temperature showing that the process is favorable at lower temperatures. The negative enthalpy change $\Delta H°$ means the adsorption process is exothermic in nature. Therefore, the higher the temperature, the lower the equilibrium constant. Furthermore, the adsorption process is a chemisorption process in nature rather than a physisorption process as the $\Delta H°$ is greater than 80 kJ/mol [61].

6. Adsorption isotherm

The adsorption isotherms are important as they provide quantitative information about the nature of solute–surface interaction, in addition to the specific relation between the concentration of adsorbate and its degree of accumulation onto adsorbent surface at constant temperature. Once equilibrium has been reached, it can be safely assumed that the concentrations of both the pollutants adsorbed to the surface and present in the water are constant, and the relation between the two is known as an adsorption isotherm [62]. Numerous models are available to study the adsorption isotherm, including the Langmuir and Freundlich models, which are used in the current research to determine the adsorption efficiency.

The Langmuir and Freundlich isotherm models were used to show the equilibrium relation for the adsorbate–adsorbent interaction. The Langmuir isotherm models monolayer coverage while the Freundlich isotherm models multilayer coverage [31]. The Langmuir isotherm model is expressed in Eq. (6) [17]:

$$\frac{C_e}{q_e} = \frac{C_e}{Q_o} + \frac{1}{K_L Q_o} \tag{6}$$

where C_e (mol/L) is the concentration of MB at equilibrium, q_e (mg/g) is the amount of adsorbate adsorbed at equilibrium, Q_o (mg/g) is the Langmuir adsorption capacity constant, and K_L (L/mg) is the Langmuir energy of adsorption constant. A graph of C_e/q_e vs. C_e (Fig. S5) was constructed and the Langmuir constants were calculated from the slope and intercept and are tabulated in Table 4. Then, the Langmuir constants were used to calculate the separation factor, R_L, which shows whether adsorption on the system is favorable or not. For it to be favorable, R_L must be between 0 and 1. The R_L for initial concentrations of 50, 150, 200, and 300 mg/L at 50 and 100 mg of HKUST-1 were calculated showing that the adsorption process is favorable in all of them (Table 5). The separation factor is calculated by Eq. (7) [17]:

Table 4
Langmuir isotherm parameters for the MB adsorption over 100 mg of HKUST-1

T (K)	Langmuir parameters			
	Q_o (mg/g)	K_L (L/mg)	K_L (L/mol)	R^2
298	66.225	1.466	468,833	0.9950
313	75.758	0.207	66,061.0	0.9837
323	108.696	0.043	13,646.0	0.9966

Table 3
Thermodynamic parameters

Temperature (K)	$1/T$ (K^{-1})	K_L (L/mol)	ln K_L	$\Delta S°$ (J/mol K)	$\Delta H°$ (J/mol)	$\Delta G°$ (J/mol)
298.15	0.00335	468,833	13.1			–32,510.7
313.15	0.00319	66,062	11.1	–267.2	–112,172.5	–28,502.9
323.15	0.00309	13,646	9.5			–25,831.0

Table 5
Isotherm constants and coefficients for 50 and 100 mg of HKUST-1

Parameter	Values	Comments
50 mg HKUST-1		
Langmuir		
Q_o (mg/g)	250	
K_L (L/mg)	0.037	
K_L (L/mol)	11,822	
R^2	0.995	
$R_{L\ 50\ mg/L}$	0.350	$0 < R < 1$ Favorable
$R_{L\ 150\ mg/L}$	0.040	
$R_{L\ 200\ mg/L}$	0.119	
$R_{L\ 300\ mg/L}$	0.082	
Freundlich		
$1/n$	0.370	$1/n < 1$ Favorable
K (L/mg)	36.448	
R^2	0.998	
100 mg HKUST-1		
Langmuir		
Q_o (mg/g)	66.225	
K_L (L/mg)	1.466	
K_L (L/mol)	468,833	
R^2	0.995	
$R_{L\ 50\ mg/L}$	0.013	$0 < R < 1$ Favorable
$R_{L\ 150\ mg/L}$	0.005	
$R_{L\ 200\ mg/L}$	0.003	
$R_{L\ 300\ mg/L}$	0.002	
Freundlich		
$1/n$	0.433	$1/n < 1$ Favorable
K (L/mg)	27.297	
R^2	0.992	

$$R_L = \frac{1}{\left(1 + K_L Q_o\right)} \tag{7}$$

The Freundlich isotherm model is as expressed in Eq. (8) [17]:

$$\ln(q_e) = \ln\left(K_f\right) + \frac{1}{n}\ln\left(C_e\right) \tag{8}$$

where K_f (mg/g) is the Freundlich constant and $1/n$ (L/mg) shows adsorption intensity and how favorable adsorption under different conditions is. If $1/n$ is less than 1, then the adsorption is favorable. A graph of ln q_e vs. ln C_e (Fig. S5(b)) was constructed and the Freundlich constants were calculated from the slope and intercept, and are tabulated in Table 5. The trend in Fig. S5(b) shows a similar plot to that of the Langmuir adsorption isotherm. However, although the data fit both the models, the R^2 for the Langmuir isotherm is higher at high adsorbent dosages (100 mg HKUST-1) while the R^2 for the Freundlich isotherm is higher at low adsorbent dosages (50 mg HKUST-1). This means that at high adsorbent dosages, the adsorption of MB better fits the Langmuir isotherm model; while at low adsorbent dosage, the adsorption of MB better fits the Freundlich isotherm model. When comparing results obtained to research done by Daneshvar et al. [49], where the adsorption of MB using brown macroalga was studied, the Langmuir adsorption capacity constant (Q_o) obtained was 95.45 mg/g which is comparable with those seen in Tables 4 and 5. However, using 50 mg of HKUST-1 obtained much higher results (250 mg/g) than the brown macroalga. Moreover, using brown macroalga obtained a $1/n$ value of 0.952 whereas when using HKUST-1, values ranging between 0.370 and 0.433 were obtained, which is more favorable for adsorption. Additionally, similar to results obtained using HKUST-1, the results obtained using brown macroalga fit both the Langmuir and Freundlich models [49]. A comparison of the constants of the Freundlich and Langmuir isotherms is depicted in Table 5 for adsorbent dosages of 50 and 100 mg.

7. Conclusion

In conclusion, experimental results show that adsorption of MB onto HKUST-1 complied well with pseudo-second-order kinetics. The optimum parameters of initial concentration, adsorbent dosage, and temperature were found to be 50 mg/L, 50 mg, and 298 K, respectively. It was found that the experimental data fit both the Langmuir model and the Freundlich model yielding a maximum adsorption capacity of 250 mg/g. However, the adsorption better fits Langmuir model at higher adsorbent dosages, while it better fits Freundlich model at lower adsorbent dosages. When the results obtained were compared with recent research being done in the field, comparable results were obtained. However, it was also noticed that using HKUST-1 as the adsorbent yielded exceptional results. Finally, the thermodynamics study indicated that the adsorption process is exothermic, spontaneous, chemisorption in nature, and that it disfavors randomness at the interface.

Acknowledgments

The authors would like to acknowledge the support received by the American University of Sharjah funds, the AUS Chemical Engineering Department funds and Faculty Research Grants FRG15-R-41.

References

[1] Y. Luo, W. Guo, H.H. Ngo, L.D. Nghiem, F.I. Hai, J. Zhang, S. Liang, X.C. Wang, A review on the occurrence of micropollutants in the aquatic environment and their fate and removal during wastewater treatment, Sci. Total Environ., 473 (2014) 619–641.
[2] D. Ragab, H.G. Gomaa, R. Sabouni, M. Salem, M. Ren, J. Zhu, Micropollutants removal from water using microfiltration membrane modified with ZIF-8 metal organic frameworks (MOFs), Chem. Eng. J., 300 (2016) 273–279.
[3] M.R. Servos, D.T. Bennie, B.K. Burnison, A. Jurkovic, R. McInnis, T. Neheli, A. Schnell, P. Seto, S.A. Smyth, T.A. Ternes, Distribution of estrogens, 17β-estradiol and estrone, in Canadian municipal wastewater treatment plants, Sci. Total Environ., 336 (2005) 155–170.

[4] F. Gagné, C. Blaise, M. Fournier, P.D. Hansen, Effects of selected pharmaceutical products on phagocytic activity in *Elliptio complanata* mussels, Comp. Biochem. Physiol. C: Toxicol. Pharmacol., 143 (2006) 179–186.
[5] N. Bolong, A.F. Ismail, M.R. Salim, T. Matsuura, A review of the effects of emerging contaminants in wastewater and options for their removal, Desalination, 239 (2009) 229–246.
[6] A. Joss, S. Zabczynski, A. Göbel, B. Hoffmann, D. Löffler, C.S. McArdell, T.A. Ternes, A. Thomsen, H. Siegrist, Biological degradation of pharmaceuticals in municipal wastewater treatment: proposing a classification scheme, Water Res., 40 (2006) 1686–1696.
[7] G.R. Boyd, H. Reemtsma, D.A. Grimm, S. Mitra, Pharmaceuticals and personal care products (PPCPs) in surface and treated waters of Louisiana, USA and Ontario, Canada, Sci. Total Environ., 311 (2003) 135–149.
[8] V. Matamoros, C. Arias, H. Brix, J.M. Bayona, Preliminary screening of small-scale domestic wastewater treatment systems for removal of pharmaceutical and personal care products, Water Res., 43 (2009) 55–62.
[9] J. Mateo-Sagasta, L. Raschid-Sally, A. Thebo, Global Wastewater and Sludge Production, Treatment and Use, in: P. Drechsel, M. Qadir, D. Wichelns, Eds., Wastewater: Economic Asset in an Urbanizing World, Springer Netherlands, Dordrecht, 2015, pp. 15–38.
[10] D. Hayelom, G. Nigus, A. Adhena, Removal of Methylene Blue Dye from textile wastewater using activated carbon prepared from rice husk, IJIAS, 9 (2014) 317–325.
[11] M.A. Barakat, New trends in removing heavy metals from industrial wastewater, Arab. J. Chem., 4 (2011) 361–377.
[12] J.-j. Gao, Y.-b. Qin, T. Zhou, D.-d. Cao, P. Xu, D. Hochstetter, Y.-f. Wang, Adsorption of methylene blue onto activated carbon produced from tea (*Camellia sinensis* L.) seed shells: kinetics, equilibrium, and thermodynamics studies, J. Zhejiang Univ. Sci. B, 14 (2013) 650–658.
[13] M. Mehrjouei, S. Müller, D. Möller, A review on photocatalytic ozonation used for the treatment of water and wastewater, Chem. Eng. J., 263 (2015) 209–219.
[14] B. Kasprzyk-Hordern, M. Ziółek, J. Nawrocki, Catalytic ozonation and methods of enhancing molecular ozone reactions in water treatment, Appl. Catal., B, 46 (2003) 639–669.
[15] A. Dąbrowska, B.K. Hordern, J. Nawrocki, Aldehydes formation during water disinfection by ozonation and chlorination process, Global Nest J., 7 (2005) 61–71.
[16] H. Dong, G. Zeng, L. Tang, C. Fan, C. Zhang, X. He, Y. He, An overview on limitations of TiO_2-based particles for photocatalytic degradation of organic pollutants and the corresponding countermeasures, Water Res., 79 (2015) 128–146.
[17] D. Pathania, S. Sharma, P. Singh, Removal of methylene blue by adsorption onto activated carbon developed from *Ficus carica* bast, Arab. J. Chem., 10 (2017) S1445–S1451.
[18] S.K. Theydan, M.J. Ahmed, Adsorption of methylene blue onto biomass-based activated carbon by $FeCl_3$ activation: equilibrium, kinetics, and thermodynamic studies, J. Anal. Appl. Pyrolysis, 97 (2012) 116–122.
[19] Z. Sun, C. Li, D. Wu, Removal of methylene blue from aqueous solution by adsorption onto zeolite synthesized from coal fly ash and its thermal regeneration, J. Chem. Technol. Biotechnol., 85 (2010) 845–850.
[20] A.H. Jawad, R.A. Rashid, R.M.A. Mahmuod, M.A.M. Ishak, N.N. Kasim, K. Ismail, Adsorption of methylene blue onto coconut (*Cocos nucifera*) leaf: optimization, isotherm and kinetic studies, Desal. Wat. Treat., 57 (2016) 8839–8853.
[21] C.-H. Weng, Y.-T. Lin, T.-W. Tzeng, Removal of methylene blue from aqueous solution by adsorption onto pineapple leaf powder, J. Hazard. Mater., 170 (2009) 417–424.
[22] J.-R. Li, R.J. Kuppler, H.-C. Zhou, Selective gas adsorption and separation in metal-organic frameworks, Chem. Soc. Rev., 38 (2009) 1477–1504.
[23] J. Lee, O.K. Farha, J. Roberts, K.A. Scheidt, S.T. Nguyen, J.T. Hupp, Metal-organic framework materials as catalysts, Chem. Soc. Rev., 38 (2009) 1450–1459.
[24] P. Horcajada, T. Chalati, C. Serre, B. Gillet, C. Sebrie, T. Baati, J.F. Eubank, D. Heurtaux, P. Clayette, C. Kreuz, J.-S. Chang, Y.K. Hwang, V. Marsaud, P.-N. Bories, L. Cynober, S. Gil, G. Ferey, P. Couvreur, R. Gref, Porous metal-organic-framework nanoscale carriers as a potential platform for drug delivery and imaging, Nat. Mater., 9 (2010) 172–178.
[25] S. Bourrelly, P.L. Llewellyn, C. Serre, F. Millange, T. Loiseau, G. Férey, Different adsorption behaviors of methane and carbon dioxide in the isotypic nanoporous metal terephthalates MIL-53 and MIL-47, J. Am. Chem. Soc., 127 (2005) 13519–13521.
[26] E. Haque, N.A. Khan, J.H. Park, S.H. Jhung, Synthesis of a metal–organic framework material, iron terephthalate, by ultrasound, microwave, and conventional electric heating: a kinetic study, Chem. Eur. J., 16 (2010) 1046–1052.
[27] L. Zhu, D. Sheng, C. Xu, X. Dai, M.A. Silver, J. Li, P. Li, Y. Wang, Y. Wang, L. Chen, C. Xiao, J. Chen, R. Zhou, C. Zhang, O.K. Farha, Z. Chai, T.E. Albrecht-Schmitt, S. Wang, Identifying the recognition site for selective trapping of $^{99}TcO_4^-$ in a hydrolytically stable and radiation resistant cationic metal–organic framework, J. Am. Chem. Soc., 139 (2017) 14873–14876.
[28] Y. Li, Z. Yang, Y. Wang, Z. Bai, T. Zheng, X. Dai, S. Liu, D. Gui, W. Liu, M. Chen, L. Chen, J. Diwu, L. Zhu, R. Zhou, Z. Chai, T.E. Albrecht-Schmitt, S. Wang, A mesoporous cationic thorium-organic framework that rapidly traps anionic persistent organic pollutants, Nat. Commun., 8 (2017) 1354.
[29] T. Zheng, Z. Yang, D. Gui, Z. Liu, X. Wang, X. Dai, S. Liu, L. Zhang, Y. Gao, L. Chen, D. Sheng, Y. Wang, J. Diwu, J. Wang, R. Zhou, Z. Chai, T.E. Albrecht-Schmitt, S. Wang, Overcoming the crystallization and designability issues in the ultrastable zirconium phosphonate framework system, Nat. Commun., 8 (2017) 15369.
[30] L. Shi, L. Hu, J. Zheng, M. Zhang, J. Xu, Adsorptive removal of methylene blue from aqueous Solution using a Ni-metal organic framework material, J. Dispersion Sci. Technol., 37 (2016) 1226–1231.
[31] E. Haque, J.W. Jun, S.H. Jhung, Adsorptive removal of methyl orange and methylene blue from aqueous solution with a metal-organic framework material, iron terephthalate (MOF-235), J. Hazard. Mater., 185 (2011) 507–511.
[32] A.A. Mohammadi, A. Alinejad, B. Kamarehie, S. Javan, A. Ghaderpoury, M. Ahmadpour, M. Ghaderpoori, Metal-organic framework Uio-66 for adsorption of methylene blue dye from aqueous solutions, Int. J. Environ. Sci. Technol., 14 (2017) 1959–1968.
[33] M. Saghanejhad Tehrani, R. Zare-Dorabei, Highly efficient simultaneous ultrasonic-assisted adsorption of methylene blue and rhodamine B onto metal organic framework MIL-68(Al): central composite design optimization, RSC Adv., 6 (2016) 27416–27425.
[34] J. Gooding, R.G. Compton, C. Brennan, J. Atherton, The dyeing of nylon and cotton cloth with azo dyes: kinetics and mechanism, J. Colloid Interface Sci., 180 (1996) 605–613.
[35] A. Nimibofa, A. Ebelegi, Wankasi, W. Donbebe, Comparative sorption studies of dyes and metal ions by Ni/Al-layered double hydroxide, Int. J. Mater. Prod. Technol., 7 (2017) 25–35.
[36] Z. Anfar, R. El Haouti, S. Lhanafi, M. Benafqir, Y. Azougarh, N. El Alem, Treated digested residue during anaerobic co-digestion of Agri-food organic waste: Methylene blue adsorption, mechanism and CCD-RSM design, J. Environ. Chem. Eng., 5 (2017) 5857–5867.
[37] M.K. Bhunia, J.T. Hughes, J.C. Fettinger, A. Navrotsky, Thermochemistry of paddle wheel MOFs: Cu-HKUST-1 and Zn-HKUST-1, Langmuir, 29 (2013) 8140–8145.
[38] S. Najafi Nobar, Cu-BTC synthesis, characterization and preparation for adsorption studies, Mater. Chem. Phys., 213 (2018) 343–351.
[39] S. Loera-Serna, H. Solis, E. Ortiz, A.L. Martínez-Hernandéz, L. Noreña, Elimination of Methylene Blue and Reactive Black 5 from aqueous solution using HKUST-1, Int. J. Environ. Sci. Technol., 8 (2017) 241–246.

[40] M.A. Zazouli, A. Azari, S. Dehghan, R. Salmani Malekkolae, Adsorption of methylene blue from aqueous solution onto activated carbons developed from eucalyptus bark and *Crataegus oxyacantha* core, Water Sci. Technol., 74 (2016) 2021.
[41] M.K. Sahu, S. Mandal, S.S. Dash, P. Badhai, R.K. Patel, Removal of Pb(II) from aqueous solution by acid activated red mud, J. Environ. Chem. Eng., 1 (2013) 1315–1324.
[42] Y. Xia, Q. Yao, W. Zhang, L. Zhang, Z. Zhang, M. Zhao, Comparative adsorption of methylene blue by magnetic baker's yeast and EDTAD-modified magnetic baker's yeast: equilibrium and kinetic study, Arab. J. Chem., (2018).
[43] S. Lin, Z. Song, G. Che, A. Ren, P. Li, C. Liu, J. Zhang, Adsorption behavior of metal–organic frameworks for methylene blue from aqueous solution, Microporous Mesoporous Mater., 193 (2014) 27–34.
[44] A. Mathews, W.J. Weber, Jr, Effects of external mass transfer and intraparticle diffusion on adsorption rates in slurry reactors, AlChE J., 73 (1977) 166.
[45] A.B. Albadarin, M.N. Collins, M. Naushad, S. Shirazian, G. Walker, C. Mangwandi, Activated lignin-chitosan extruded blends for efficient adsorption of methylene blue, Chem. Eng. J., 307 (2017) 264–272.
[46] G. Sharma, M. Naushad, A. Kumar, S. Rana, S. Sharma, A. Bhatnagar, F.J. Stadler, A.A. Ghfar, M.R. Khan, Efficient removal of coomassie brilliant blue R-250 dye using starch/poly(alginic acid-cl-acrylamide) nanohydrogel, Process Saf. Environ. Prot., 109 (2017) 301–310.
[47] A.A. Alqadami, M. Naushad, Z.A. Alothman, T. Ahamad, Adsorptive performance of MOF nanocomposite for methylene blue and malachite green dyes: kinetics, isotherm and mechanism, J. Environ. Manage., 223 (2018) 29–36.
[48] A. Boukhemkhem, K. Rida, Improvement adsorption capacity of methylene blue onto modified Tamazert kaolin, Adsorpt. Sci. Technol., 35 (2017) 753–773.
[49] E. Daneshvar, A. Vazirzadeh, A. Niazi, M. Kousha, M. Naushad, A. Bhatnagar, Desorption of Methylene blue dye from brown macroalga: effects of operating parameters, isotherm study and kinetic modeling, J. Cleaner Prod., 152 (2017) 443–453.
[50] J. Chang, J. Ma, Q. Ma, D. Zhang, N. Qiao, M. Hu, H. Ma, Adsorption of methylene blue onto Fe_3O_4/activated montmorillonite nanocomposite, Appl. Clay Sci., 119 (2016) 132–140.
[51] E.I. El-Shafey, S.N.F. Ali, S. Al-Busafi, H.A.J. Al-Lawati, Preparation and characterization of surface functionalized activated carbons from date palm leaflets and application for methylene blue removal, J. Environ. Chem. Eng., 4 (2016) 2713–2724.
[52] K.T. Wong, N.C. Eu, S. Ibrahim, H. Kim, Y. Yoon, M. Jang, Recyclable magnetite-loaded palm shell-waste based activated carbon for the effective removal of methylene blue from aqueous solution, J. Cleaner Prod., 115 (2016) 337–342.
[53] J. Hu, L. Liu, Z. Xiao, Adsorptions of Cd(ii) and methylene blue from aqueous solution by silica hybrid hollow spheres, RSC Adv., 5 (2015) 68092–68098.
[54] J. Fu, Z. Chen, M. Wang, S. Liu, J. Zhang, J. Zhang, R. Han, Q. Xu, Adsorption of methylene blue by a high-efficiency adsorbent (polydopamine microspheres): kinetics, isotherm, thermodynamics and mechanism analysis, Chem. Eng. J., 259 (2015) 53–61.
[55] J. Feng, Y. Wang, L. Zou, B. Li, X. He, Y. Ren, Y. Lv, Z. Fan, Synthesis of magnetic ZnO/$ZnFe_2O_4$ by a microwave combustion method, and its high rate of adsorption of methylene blue, J. Colloid Interface Sci., 438 (2015) 318–322.
[56] T. Shen, J. Luo, S. Zhang, X. Luo, Hierarchically mesostructured MIL-101 metal–organic frameworks with different mineralizing agents for adsorptive removal of methyl orange and methylene blue from aqueous solution, J. Environ. Chem. Eng., 3 (2015) 1372–1383.
[57] Y. Liu, Y.-J. Liu, Biosorption isotherms, kinetics and thermodynamics, Sep. Purif. Technol., 61 (2008) 229–242.
[58] Y. Liu, H. Xu, Equilibrium, thermodynamics and mechanisms of Ni^{2+} biosorption by aerobic granules, Biochem. Eng. J., 35 (2007) 174–182.
[59] Y. Liu, Is the free energy change of adsorption correctly calculated?, J. Chem. Eng. Data, 54 (2009) 1981–1985.
[60] É.C. Lima, M.A. Adebayo, F.M. Machado, Kinetic and Equilibrium Models of Adsorption, in: C.P. Bergmann, F.M. Machado, Eds., Carbon Nanomaterials as Adsorbents for Environmental and Biological Applications, Springer International Publishing, Switzerland, 2015, pp. 33–69.
[61] V.J. Inglezakis, A.A. Zorpas, Heat of adsorption, adsorption energy and activation energy in adsorption and ion exchange systems, Desal. Wat. Treat., 39 (2012) 149–157.
[62] K. Li, X. Wang, Adsorptive removal of Pb(II) by activated carbon prepared from *Spartina alterniflora*: equilibrium, kinetics and thermodynamics, Bioresour. Technol., 100 (2009) 2810-2815.

Supplementary figures

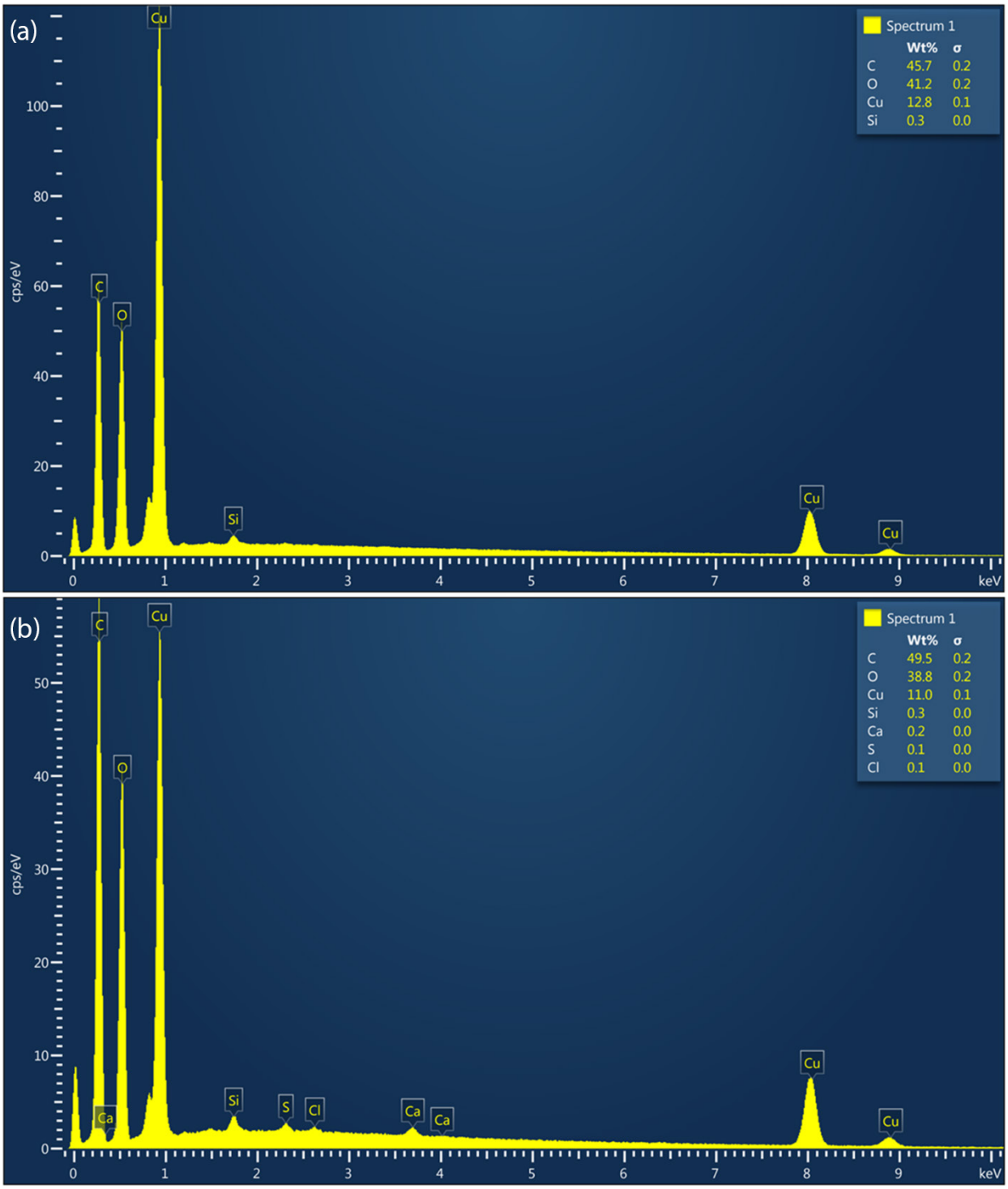

Fig. S1. EDX images of HKUST-1 (a) and HKUST-1 after adsorption of MB (b).

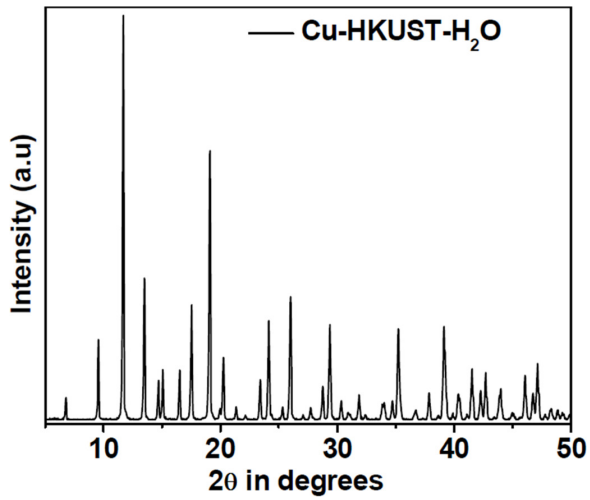

Fig. S2. Simulated XRD of HKUST-1 based on a study by Bhunia et al. [37].

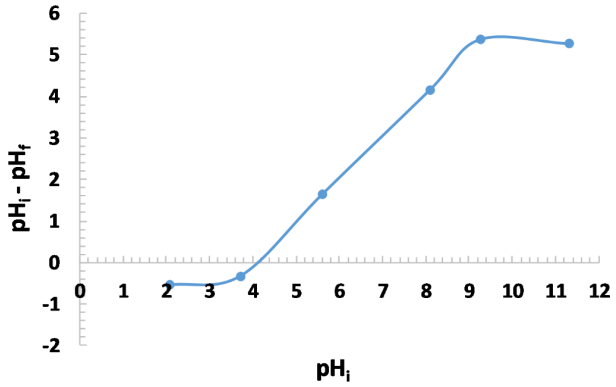

Fig. S3. Point of zero charge of HKUST-1.

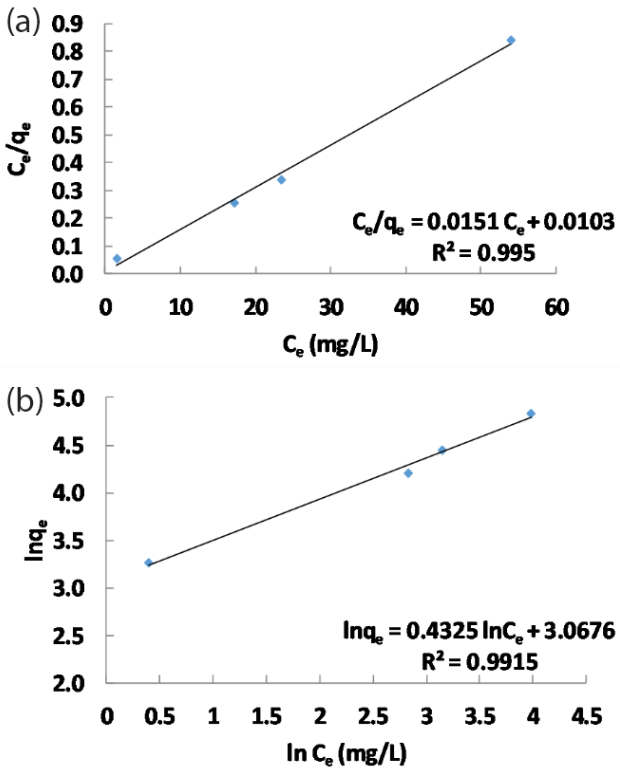

Fig. S5. (a) Langmuir isotherm model for 100 mg of HKUST-1, (b) Freundlich isotherm model for 100 mg HKUST-1.

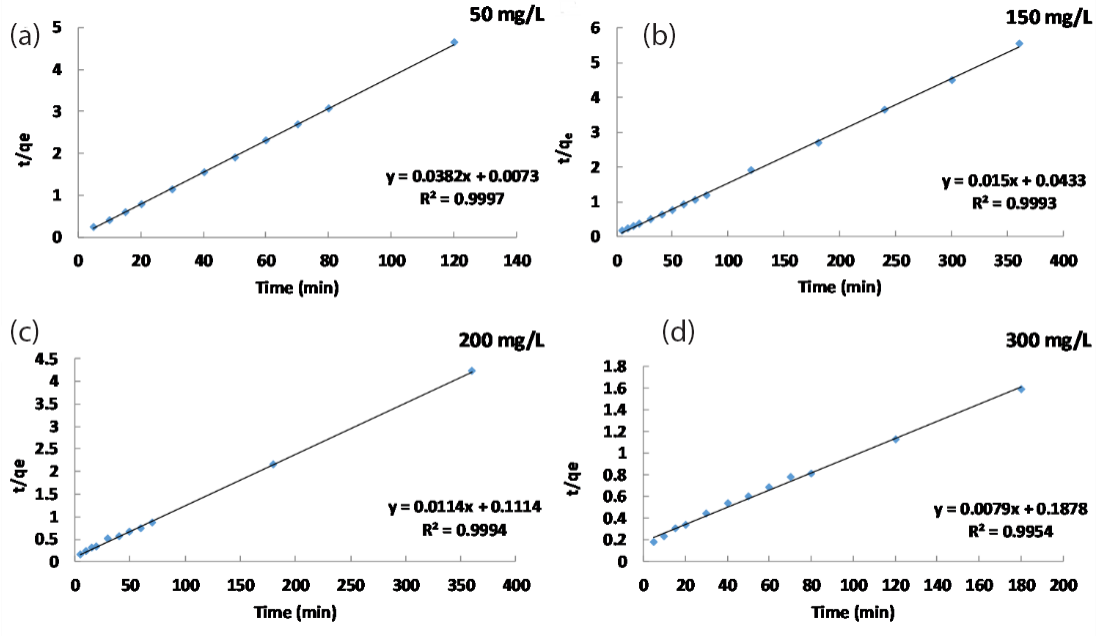

Fig. S4. Pseudo-second-order plot for removal of MB by 100 mg of HKUST-1.